第 43 卷 第 4 期/2023 年 2 月/光学学报 研究论文

光学学报

光伏型HgCdTe阵列探测器的电学串扰

乔帅[1,2,3]，王睿[1,2,3*]，侯孝成[1,2,3]

[1]国防科技大学前沿交叉学科学院，湖南 长沙 410073；

[2]国防科技大学南湖之光实验室，湖南 长沙 410073；

[3]国防科技大学脉冲功率激光技术国家重点实验室，湖南 长沙 410073

摘要 阵列探测器单元间的串扰是影响探测效果的重要因素，研究探测器的串扰机理及其抑制措施有助于优化探测器性能。针对激光辐照线阵HgCdTe探测器实验中的串扰现象，使用COMSOL Multiphysics有限元仿真软件建立了激光辐照探测器的三维仿真模型，通过模拟芯片内载流子浓度分布、光电流和电场，揭示了电学串扰的产生机理，并针对该器件提出了沟槽隔离的抑制串扰措施。研究结果表明：光生载流子沿线阵排列方向的横向扩散是造成被辐照像元附近像元串扰的直接因素，但对距离辐照区域较远的像元影响较小；公共P极电压降低是导致距离辐照区域较远的像元产生响应的根本原因。此外，仿真结果验证了提出的沟槽隔离措施对电学串扰具有显著的抑制效果。

关键词 探测器；HgCdTe；电学串扰；串扰机理；沟槽隔离

中图分类号 TN215 **文献标志码** A **DOI**：10.3788/AOS221555

1 引 言

红外探测技术可将人眼不可见的红外辐射可视化，被广泛应用于民用、军事领域。至今，红外探测技术经历了三代技术革新，从第一代的单元、小线阵光电导探测器，到第二代的焦平面阵列器件，再到如今第三代的大面阵、多波段探测器[1]。近年来，二维材料的发展为新一代红外探测器的创新打开了新局面[2-7]。

随着探测器阵列规模的增大，像元中心距不断减小，探测器的空间分辨率得到了提升，但串扰效应也变得更加突出，此时其对探测器的性能会产生不可忽略的影响[8-10]。串扰效应指本应在目标像元产生的信号受到某种因素干扰使其他像元产生了响应信号。根据产生机制的不同可以将串扰分为光学串扰和电学串扰：光学串扰指因光的反射、折射、衍射等光学因素使信号出现在其他像元中[11]；电学串扰指因光生载流子的扩散导致其他像元处出现信号响应[12]。

HgCdTe探测器因其灵敏度高、覆盖波段范围广等一系列优点成为第三代红外探测器的主流[13-14]。目前，有关阵列型HgCdTe探测器的激光辐照效应已有大量研究，发现该类探测器在连续激光和脉冲激光的作用下均存在串扰现象[15-16]。文献[17-19]研究了光学串扰对线阵探测器输出的影响，发现光学串扰并非造成线阵器件未被辐照像元响应的主要因素，而是电路结构。文献[20]通过实验证实了光学因素并非不同通道单元间产生串扰的来源，推断未被辐照像元的响应是由电学串扰导致的，但尚未对该结论进行系统的分析验证。本文针对线阵HgCdTe探测器的串扰现象，研究了该器件电学串扰的机理和串扰程度，并探索了抑制电学串扰的有效措施，为探测器性能优化提供了参考。

2 实验及结果

2.1 探测器工作原理

选择512×1线阵HgCdTe探测器为研究对象，探测器芯片封装于液氮制冷的真空杜瓦瓶内，工作温度为77 K，响应波段为1～3 μm。该探测器共512个光敏像元，且呈奇偶两列并行排布于光敏芯片上，像元尺寸为28 μm×28 μm，相邻像元中心距为56 μm。公共电极P极位于光敏元阵列两侧，用于施加偏置电压，采用背照射式结构接收红外辐射信号，如图1所示。

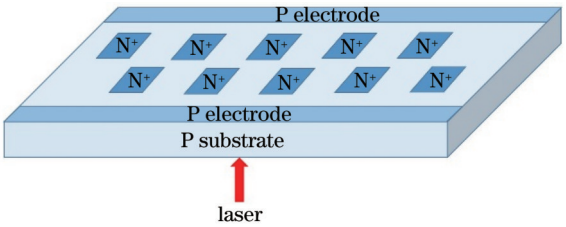

图1 光敏元阵列示意图

Fig. 1 Schematic diagram of photosensitive element array

收稿日期：2022-08-01；**修回日期**：2022-08-25；**录用日期**：2022-09-21；**网络首发日期**：2022-09-30

通信作者：*xi_g_z@126.com

该探测器的每个像元通过铟柱与读出电路间接相连，将接收到的光信号转化成电信号并通过读出电路输出。读出电路采用电容反馈跨阻放大器(CTIA)结构，如图 2 所示。其中，V_{in}为光电流输入端处的电压，I为输入电流，V_{ref}为公共参考电压(通常设为 2 V)，C_{int}为积分电容的大小，输出端与后处理电路相连并将信号以电压形式输出(V_{out})。

2.2　实验光路

实验使用波长为 1064 nm、脉冲宽度为 15 ps 的单脉冲激光辐照线阵 HgCdTe 探测器。采用衰减片组合控制激光能量密度，利用小孔光阑控制激光光斑大小，利用码型发生器控制激光器和探测器的工作时序，确保激光入射在探测器的积分时间段内，并利用示波器来测量探测器的输出电压信号。实验光路示意图如图 3 所示。

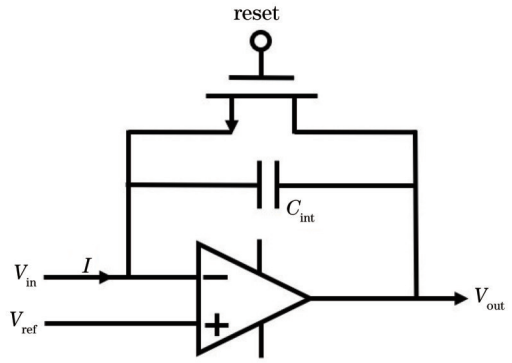

图 2　CTIA 结构示意图

Fig. 2　Structural diagram of CTIA

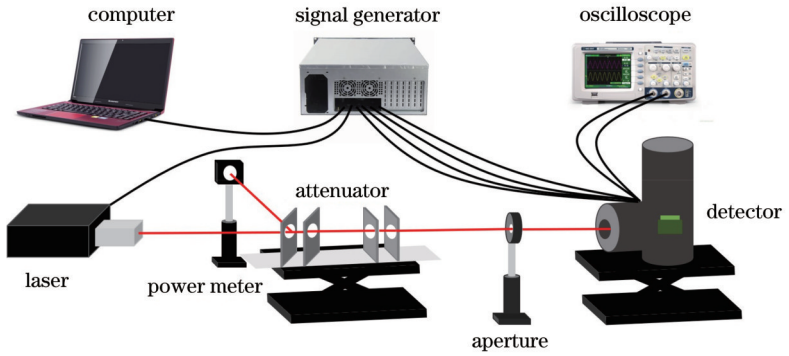

图 3　实验光路示意图

Fig. 3　Schematic diagram of experimental optical path

2.3　实验结果

测量不同能量密度激光辐照下被辐照像元和距离辐照区较远的某一未被辐照像元的光响应信号，结果如图 4 所示。可以看出：随着激光能量的增大，被辐照像元的光响应信号先线性增大，再达到饱和电压值(约 3.5 V)；未被辐照像元也存在响应，增大至 2 V 左右后不再有明显变化。该实验现象表明，距离辐照区较远的像元处会存在明显的串扰，但存在串扰的像元的响应值会受到某种限制而不会超过被辐照像元的响应值。

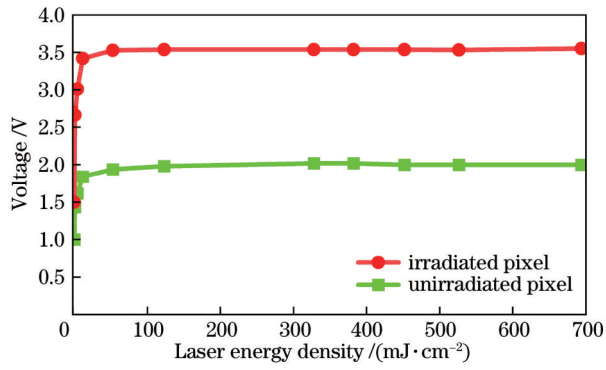

图 4　被辐照与未被辐照像元在不同能量激光辐照下的响应

Fig. 4　Response of irradiated and unirradiated pixels under laser irradiation with different energies

3　建模与分析

3.1　理论模型

通常使用漂移-扩散模型描述光生载流子的输运规律。基于传统的漂移-扩散模型[21]，考虑浓度梯度和温度梯度的影响，将电子和空穴的电流密度方程拓展为

$$J_n = qn\mu_n\nabla E_c + qD_n\nabla n - qnD_n\nabla(\ln N_c) + qnD_{n,th}\nabla(\ln T), \quad (1)$$

$$J_p = qp\mu_p\nabla E_v + qD_p\nabla p + qpD_p\nabla(\ln N_v) - qpD_{p,th}\nabla(\ln T), \quad (2)$$

式中：J_n和J_p分别为电子和空穴的电流密度；n和p分别为电子和空穴的密度；q为电子电量；E_c和E_v分别为导带底和价带顶的能量；N_c和N_v分别为导带和价带的有效状态密度；μ_n和μ_p分别为电子和空穴的迁移率；D_n和D_p分别为电子和空穴的扩散系数；$D_{n,th}$和$D_{p,th}$分别为电子和空穴的热扩散系数；T为温度。

电子和空穴在探测器内的输运遵循的连续性方程[21]为

$$q\frac{\partial n}{\partial t}=\nabla\cdot\boldsymbol{J}_n, \tag{3}$$

$$q\frac{\partial p}{\partial t}=\nabla\cdot\boldsymbol{J}_p, \tag{4}$$

电场变化遵循泊松方程[22]

$$\nabla\cdot\boldsymbol{E}=\frac{q}{\varepsilon}\left(N_{\mathrm{D}}-N_{\mathrm{A}}+p-n\right), \tag{5}$$

式中：ε为材料的相对介电常数；N_{D}和N_{A}分别为施主杂质浓度和受主杂质浓度。

求解漂移扩散方程可得到载流子浓度和电流密度，进而得到通过像元的光电流大小。将电学串扰的串扰率定义为近邻未被辐照像元的平均光电流与被辐照中心像元的光电流的比值[23]，即

$$R=\left(\frac{\frac{1}{N}\sum_{N}I_{\mathrm{ph}}}{I_{\mathrm{ph0}}}\right)\times 100\%, \tag{6}$$

式中：I_{ph0}为完全被辐照像元产生的光电流；I_{ph}为近邻未被辐照像元产生的光电流；N为近邻未被辐照像元的数量。

3.2　建立物理模型

基于载流子输运的漂移扩散理论，使用COMSOL Multiphysics有限元仿真软件建立激光辐照探测器芯片的三维仿真模型，模型示意图如图5所示。施加波长为1064 nm、脉冲宽度为15 ps的单脉冲激光于探测器芯片上。其中，5号和6号像元完全被辐照，4号和7号像元部分被辐照，其余像元均未被辐照。在该模型中，根据式(6)将3号像元与5号像元光电流的比值作为电学串扰率。

模型中的读出电路如图6所示，其中V_{bias}为放大电路的偏置电压(3.55 V)，V_{dd}为放大电路的电源电压(5 V)。公共电极P极处施加的偏置电压V_{b}为2 V，光敏元N区与CTIA电路相连，CTIA电路中的放大器采用五管放大结构[24]。

光敏元流入电路的电流I由光电流I_{p}和暗电流I_{d}两部分组成，即

$$I=I_{\mathrm{p}}-I_{\mathrm{d}}, \tag{7}$$

$$I_{\mathrm{d}}=I_0\left[\exp\left(q\frac{V_{\mathrm{b}}-V_{\mathrm{ref}}}{kT}\right)\right], \tag{8}$$

电路中放大器的输出电压为

$$V_{\mathrm{out}}=V_{\mathrm{ref}}-\frac{It_{\mathrm{int}}}{C_{\mathrm{int}}}, \tag{9}$$

式中：I_0为反向饱和电流；k为玻尔兹曼常数；t_{int}为积分时间。

将式(7)和式(8)代入式(9)中可得

$$V_{\mathrm{out}}=V_{\mathrm{ref}}+\frac{I_{\mathrm{p}}t_{\mathrm{int}}}{C_{\mathrm{int}}}-\frac{I_0\left[\exp\left(q\frac{V_{\mathrm{b}}-V_{\mathrm{ref}}}{kT}\right)-1\right]t_{\mathrm{int}}}{C_{\mathrm{int}}}, \tag{10}$$

在探测器实际应用中，为降低暗电流，通常令$V_{\mathrm{b}}=V_{\mathrm{ref}}$，从而使探测器处于零偏工作状态[18]。

3.3　电学串扰机理分析

通过模拟光敏芯片内部载流子浓度的空间分布(以电子为例)随激光入射时间的变化情况，定性观察载流子的扩散情况。当激光能量密度为150 mJ/cm^{2}时，载流子浓度在空间分布的变化如图7所示。图7(a)为激光未辐照时半导体平衡态下的载流子浓度分布情况。图7(b)为激光辐照时的载流子浓度分布。图7(c)～(f)展示了激光脉冲结束后载流子浓度分布随时间的变化情况。

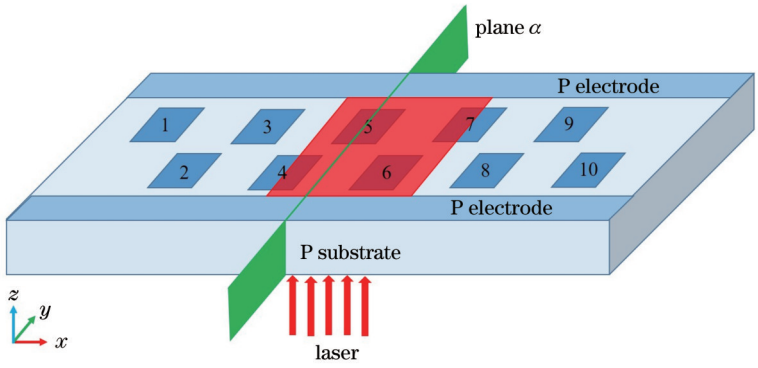

图5　激光辐照探测器示意图

Fig. 5　Schematic diagram of detector irradiated by laser

仿真结果表明：受单脉冲激光辐照后，首先在P衬底被辐照表面上产生大量光生载流子，随着时间的推移沿z正方向扩散，扩散至PN结的载流子被内建电场分离并通过外部电路形成光电流；在相邻像元之间没有外部电路的区域中，光生载流子会不断累积，并沿x方向横向扩散至未辐照区域，使其他像元处产生串扰；随着时间的推移，光生载流子逐渐复合恢复到光照前的半导体平衡态。该能量激光辐照下5号像元的光电流大小为1.24 A，因x方向扩散的光生载流子而造成的3号像元处产生的光电流大小为0.4 A，由式(6)可得串扰率为32.3%。

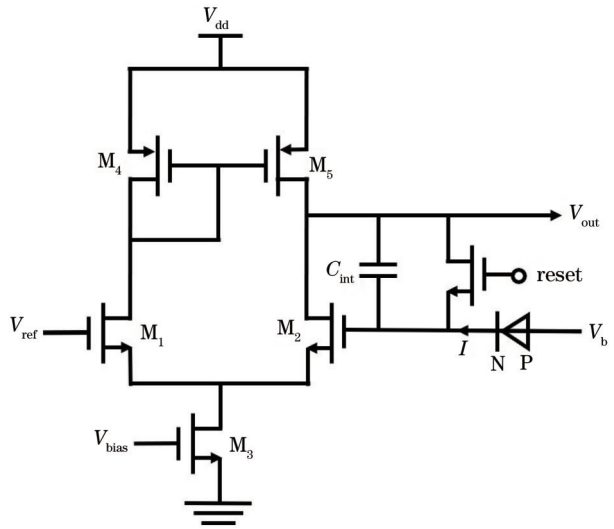

图 6　模型中的读出电路示意图

Fig. 6　Schematic diagram of readout circuit in model

3.3.1　沿 x 方向的串扰

通过模拟各像元中心的载流子浓度，对不同能量激光辐照下的载流子扩散程度进行定量研究。该器件结构沿 x 方向高度对称，故只考虑 1～5 号像元。当激光能量密度分别为 1.5、15、150、600 mJ/cm^2 时，各像元中心载流子浓度随时间的变化情况如图 8 所示。

根据图 8 所示的仿真结果可以看出：当激光能量密度为 1.5 mJ/cm^2 时，处于辐照区的 4 号和 5 号像元的载流子浓度较高，而未辐照的 1 号、2 号、3 号像元的载流子浓度几乎不变；当激光能量密度为 15 mJ/cm^2 时，3 号像元处出现明显的串扰；当激光能量密度为 150 mJ/cm^2 时，3 号像元处的串扰增强，而 1 号和 2 号像元的载流子浓度仍然保持不变；当激光能量密度为 600 mJ/cm^2 时，2 号像元处出现串扰，而 1 号像元仍无明显变化，且被辐照的 4 号和 5 号像元的载流子浓度出现“凹陷”的反常现象，该现象是由激光能量过大引起辐照区材料性质发生改变从而引起 PN 结电场方向发生变化所致。

在上述激光能量范围内，载流子在 x 方向的扩散仅会造成与 5 号像元相邻的 3 号像元处出现较明显的串扰，而对 1 号像元的影响可忽略不计，表明载流子在 x 方向的扩散对未被辐照像元的影响有限，并非造成距离辐照区较远的像元产生响应的主要因素。

3.3.2　沿 y 方向的串扰

载流子沿 y 方向的扩散在图 7 中并不能直观体现，为研究该器件在 y 方向的串扰，对图 5 中 α 平面（yz 面的平行面）的载流子浓度和电场方向进行仿真研究，如图 9 所示。

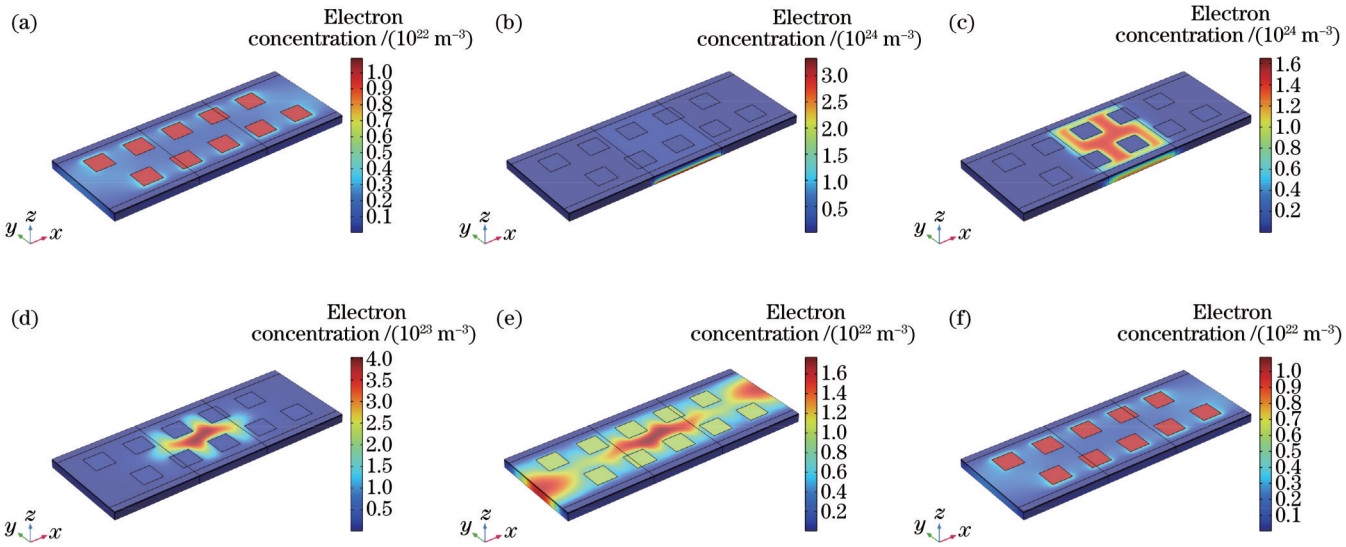

图 7　电子浓度分布随激光入射时间 t 的变化。(a) t=0；(b) t=15 ps；(c) t=30 ps；(d) t=200 ps；(e) t=1000 ps；(f) t=2000 ps

Fig. 7　Electron concentration distribution varying with laser incident time t. (a) t=0; (b) t=15 ps; (c) t=30 ps; (d) t=200 ps; (e) t=1000 ps; (f) t=2000 ps

仿真结果表明：激光辐照 P 衬底之后，存在指向两侧公共电极 P 极的电场，有部分光生载流子在该电场的作用下产生流向 P 极的电流。在电路中，向 P 极施加的偏置电压 V_b 通常为 2 V，而流向 P 极的光电流为反向电流，故会造成 P 极电压 V_b 降低。由式（10）可知：探测器理想工作情况下 V_b=V_{ref}，此时等式右边第三项为零；若 V_b 降低，而 V_{ref} 保持不变，则等式右边第三项成为不为零的负数，此时等式右边三项之和增大，从而导致输出响应上升。由于 V_b 为公共电极 P 极处的电压，故 V_b 的降低会导致探测器内所有像元的响应上升。

综上所述，器件的公共 P 极电压降低是造成距离辐照区较远的像元响应的主要因素。为验证该结论，对公共 P 极电压在不同能量激光辐照下的变化情况进

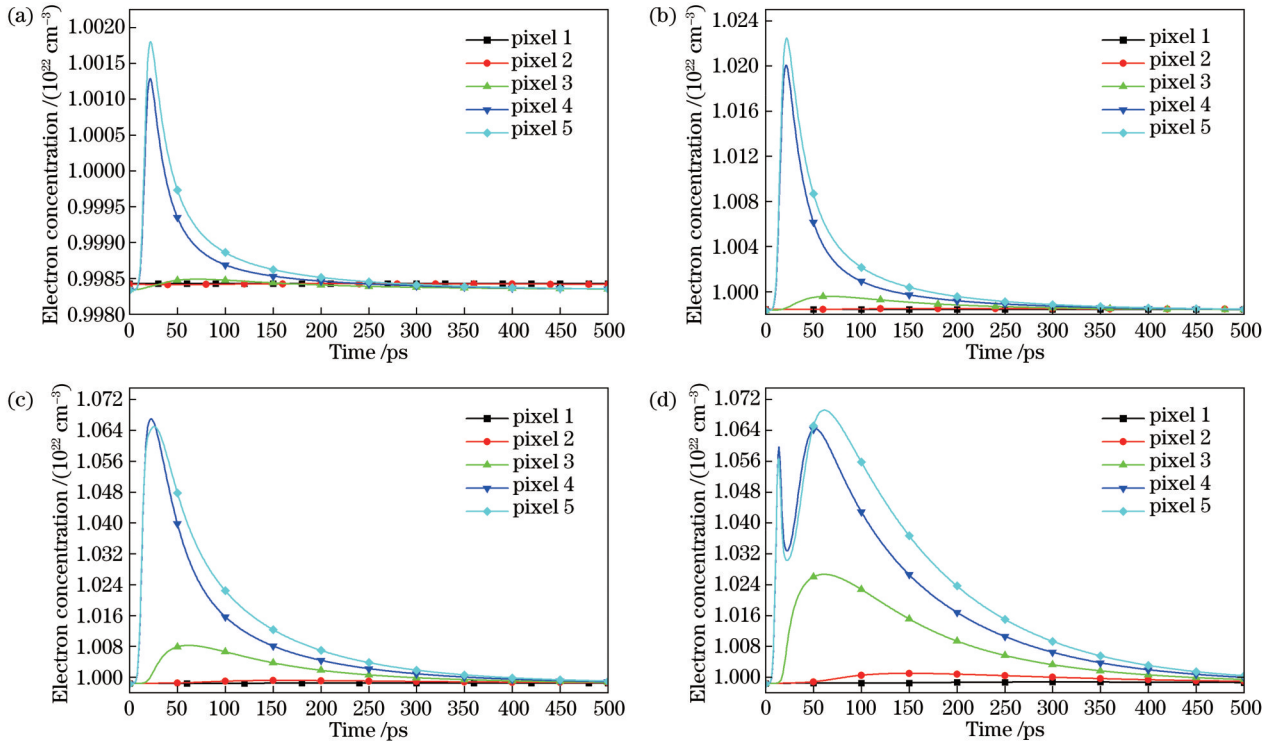

图 8　不同激光能量下各像元中心电子浓度随时间的变化情况。(a) 1.5 mJ/cm^2;(b) 15 mJ/cm^2;(c) 150 mJ/cm^2;(d) 600 mJ/cm^2

Fig. 8　Electron concentration in center of each pixel varying with time at different laser energies. (a) 1.5 mJ/cm^2; (b) 15 mJ/cm^2; (c) 150 mJ/cm^2; (d) 600 mJ/cm^2

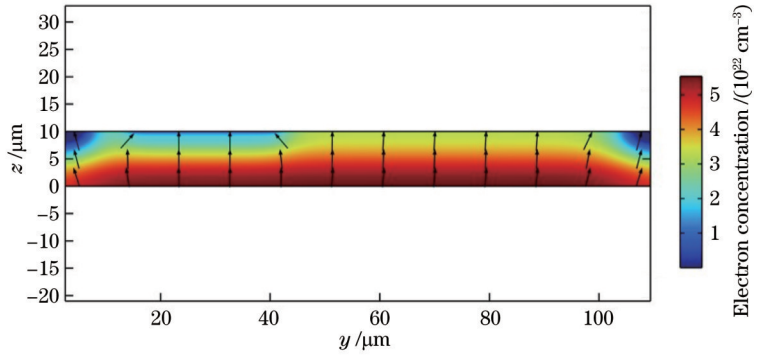

图 9　α 平面的电子浓度和电场方向

Fig. 9　Electron concentration and electric field direction of plane α

行仿真,结果如图 10 所示。

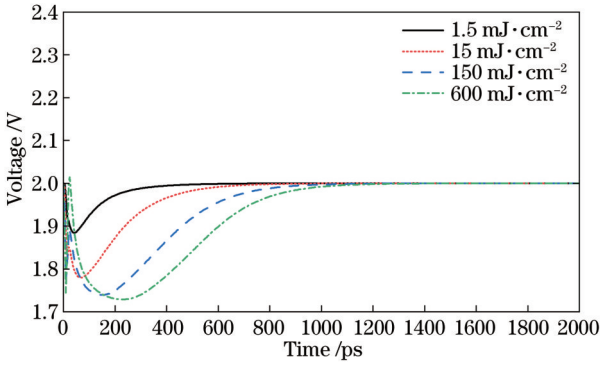

图 10　公共 P 电极电压随时间的变化

Fig. 10　Voltage of common P electrode varying with time

从仿真结果可以看出:在较低能量的激光辐照下,P 电极电压呈现先降低、后增大和在激光脉冲结束后逐渐恢复至初始 2 V 的过程;辐照激光能量越大,P 电极电压降低的幅度越大;在激光能量密度超过 150 mJ/cm^{2}后,P 电极电压不再发生显著下降,激光能量密度为 600 mJ/cm^{2}和 150 mJ/cm^{2}时的 P 电极电压最小值相比仅降低约 0.01 V。该结果表明 P 电极电压会随着入射激光能量的增大而降低,且降低到一定程度后不再有明显变化。

3.3.3　串扰机理总结

载流子在 x 方向的横向扩散是被辐照区附近像元处产生串扰的直接因素,但对距离辐照中心较远的像元的影响较小。在 y 方向上,载流子扩散到 P 电极,通

过改变P电极电压从而间接影响了输出电压，是造成距离辐照中心较远的像元处产生串扰的主要原因。P电极电压下降到一定程度后不再有明显下降的趋势，是造成未被辐照像元响应电压受到约束而不超过被辐照像元响应电压的原因。

4　电学串扰的抑制措施

基于阻止或减少载流子的横向扩散来抑制电学串扰的思路，针对该器件提出建立三维隔离沟槽的抑制串扰措施。现有文献中关于沟槽隔离方法的研究主要通过TCAD软件进行二维模拟，如在该模型中的xz平面上进行，而不考虑y方向，即默认沟槽完全贯穿y方向。然而，实际应用中无法实现沟槽在y方向上完全贯穿，沟槽在y方向的尺寸对串扰抑制效果有较大影响。本文结合器件实际结构，建立了三维沟槽隔离防串扰模型，并研究不同沟槽长度（y方向）对器件串扰率的影响。

在相邻像元之间构造长度为42 μm、宽度为1 μm、深度为10 μm的沟槽，光照参数保持不变，得到在光照结束1000 ps时刻的载流子浓度分布，如图11所示。与图7(e)相比，沟槽隔离模型中载流子的横向扩散程度有明显的改善，此时5号像元处的光电流大小为1.24 A，而串扰造成的3号像元处的光电流大小仅为0.18 A，串扰率为14.5%，与无沟槽结构相比下降了17.8个百分点。

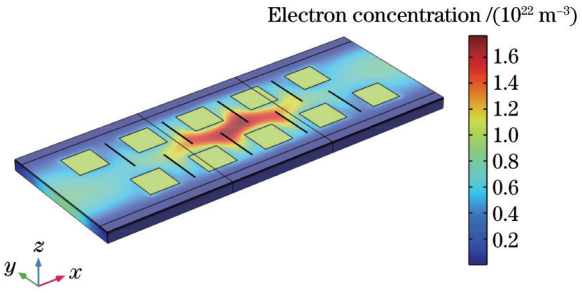

图11　沟槽隔离模型中的电子浓度分布

Fig. 11　Electron concentration distribution in trench isolation model

对不同沟槽长度的器件的串扰率进行了计算，结果如图12所示。可以看出，串扰率随着沟槽长度的增加而逐渐减小，但沟槽过大可能会导致光敏芯片机械强度低、可靠性差[25]的问题出现，在实际应用中需综合考虑串扰率与芯片可靠性，从而设计出长度合适的沟槽。

5　结　　论

针对激光辐照线阵HgCdTe探测器实验中出现的串扰现象，通过模拟光敏芯片内部载流子的浓度分布、光电流和电场，揭示了载流子的横向扩散和公共P极

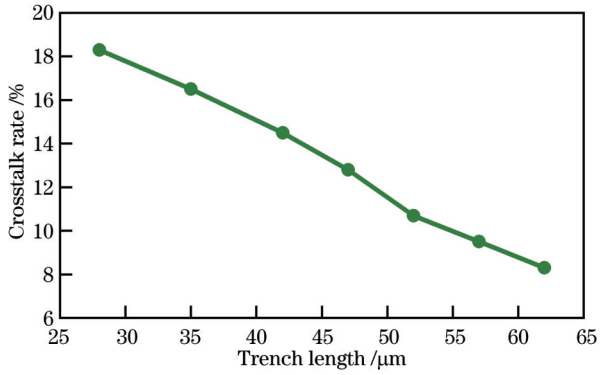

图12　串扰率随沟槽长度的变化

Fig. 12　Crosstalk rate varying with trench length

电压改变是产生电学串扰的机理，为抑制串扰措施的研究提供了思路和方向。基于载流子横向扩散造成电学串扰的机理，提出了通过沟槽隔离降低电学串扰的措施，具有显著的抑制串扰效果，为器件结构的合理设计提供了重要参考。除此之外，解决电学串扰问题的措施还有保护环结构[25]、深P阱技术[26]和金属框结构[27]等。对于公共P极电压改变造成的串扰，可通过优化电路结构或对输出信号进行校正[28]解决，具体措施有待进一步研究。

参　考　文　献

[1] 叶振华, 李辉豪, 王进东, 等. 红外光电探测器的前沿热点与变革趋势[J]. 红外与毫米波学报, 2022, 41(1): 15-39.
Ye Z H, Li H H, Wang J D, et al. Recent hotspots and innovative trends of infrared photon detectors[J]. Journal of Infrared and Millimeter Waves, 2022, 41(1): 15-39.

[2] Li Q G, Rao H, Mei H J, et al. Erbium-doped WS_2 with down- and up-conversion photoluminescence integrated on silicon for heterojunction infrared photodetection[J]. Advanced Materials Interfaces, 2022, 9(24): 2201175.

[3] 于平平, 段伟, 姜岩峰. 基于Se/TiO_2纳米纤维的自驱动光电探测器特性[J]. 光学学报, 2022, 42(14): 1404001.
Yu P P, Duan W, Jiang Y F. Photoelectric properties of self-powered photodetectors based on Se/TiO_2 nanofibers[J]. Acta Optica Sinica, 2022, 42(14): 1404001.

[4] 林亚楠, 吴亚东, 程海洋, 等. $PdSe_2$纳米线薄膜/Si异质结近红外集成光电探测器[J]. 光学学报, 2021, 41(21): 2125001.
Lin Y N, Wu Y D, Cheng H Y, et al. Near-infrared integrated photodetector based on $PdSe_2$ nanowires film/Si heterojunction [J]. Acta Optica Sinica, 2021, 41(21): 2125001.

[5] 姚杰, 缪鑫, 王帅, 等. 高响应度光电检测器件石墨烯-MoS_2垂直异质结的制备[J]. 激光与光电子学进展, 2021, 58(15): 1516024.
Yao J, Miao X, Wang S, et al. Preparation of graphene-MoS_2 vertical heterojunction for high-responsivity photodetectors[J]. Laser & Optoelectronics Progress, 2021, 58(15): 1516024.

[6] Yang X G, Li B J. Monolayer MoS_2 for nanoscale photonics[J]. Nanophotonics, 2020, 9(7): 1557-1577.

[7] Yang X G, Liu Y, Lei H X, et al. An organic-inorganic broadband photodetector based on a single polyaniline nanowire doped with quantum dots[J]. Nanoscale, 2016, 8(34): 15529-15537.

[8] Li Y, Ye Z H, Lin C, et al. Crosstalk suppressing design of GaAs microlenses integrated on HgCdTe infrared focal plane array[J]. Optical and Quantum Electronics, 2013, 45(7):

665-672.

[9] Schuster J, Bellotti E. Evaluation of quantum efficiency, crosstalk, and surface recombination in HgCdTe photon-trapping structures[J]. Journal of Electronic Materials, 2014, 43(8): 2808-2817.

[10] Vallone M, Goano M, Bertazzi F, et al. Simulation of small-pitch HgCdTe photodetectors[J]. Journal of Electronic Materials, 2017, 46(9): 5458-5470.

[11] 龙弯, 王睿, 许中杰. 红外成像系统中串扰效应的研究现状与进展[J]. 激光与光电子学进展, 2015, 52(10): 1000041.
Long W, Wang R, Xu Z J. Research status and development of crosstalk in the infrared imaging systems[J]. Laser & Optoelectronics Progress, 2015, 52(10): 1000041.

[12] 赖莉萍, 罗福, 张蓉竹. CMOS阵列响应过程中的电串扰特性研究[J]. 强激光与粒子束, 2015, 27(6): 0610191.
Lai L P, Luo F, Zhang R Z. Research on electrical crosstalk of CMOS array[J]. High Power Laser and Particle Beams, 2015, 27(6): 0610191.

[13] 蔡毅. 碲镉汞探测器的回顾与展望(特邀)[J]. 红外与激光工程, 2022, 51(1): 20210988.
Cai Y. Review and prospect of HgCdTe detectors (Invited)[J]. Infrared and Laser Engineering, 2022, 51(1): 20210988.

[14] 马润泽, 张晓明, 冯帅, 等. 红外光电探测技术研究现状及展望(特邀)[J]. 光子学报, 2021, 50(10): 1004006.
Ma R Z, Zhang X M, Feng S, et al. Research status and prospect of infrared photoelectric detection technology (invited)[J]. Acta Photonica Sinica, 2021, 50(10): 1004006.

[15] 邱伟成. 线阵光伏型碲镉汞探测器激光辐照效应若干问题研究[D]. 长沙: 国防科技大学, 2012: 14-33.
Qiu W C. Research on the irradiation effects of PV-HgCdTe linear array detector under laser[D]. Changsha: National University of Defense Technology, 2012: 14-33.

[16] 张月. 线阵碲镉汞探测器对短脉冲激光的反常响应机理研究[D]. 长沙: 国防科技大学, 2017.
Zhang Y. Researches on the abnormal response of PV-HgCdTe linear array detector induced by short pulse laser[D]. Changsha: National University of Defense Technology, 2017.

[17] 邱伟成, 王睿, 许中杰, 等. PV型HgCdTe线阵探测器的光学串扰[J]. 强激光与粒子束, 2012, 24(10): 2325-2330.
Qiu W C, Wang R, Xu Z J, et al. Optical crosstalk of HgCdTe PV linear array detector[J]. High Power Laser and Particle Beams, 2012, 24(10): 2325-2330.

[18] 邱伟成, 王睿, 江天, 等. PV型HgCdTe线阵探测器对强光反常响应机制研究[J]. 光学学报, 2012, 32(10): 1004001.
Qiu W C, Wang R, Jiang T, et al. Study of unusual response mechanism to PV HgCdTe linear array detector by hard light[J]. Acta Optica Sinica, 2012, 32(10): 1004001.

[19] 邱伟成, 王睿, 许中杰, 等. 基于CTIA的PV-HgCdTe线阵近红外激光响应特性[J]. 红外与激光工程, 2013, 42(6): 1394-1398.
Qiu W C, Wang R, Xu Z J, et al. Study on the light response characteristics of PV HgCdTe linear array detector with CTIA circuit[J]. Infrared and Laser Engineering, 2013, 42(6): 1394-1398.

[20] 龙弯. 光伏型红外TDI阵列碲镉汞探测器的串扰机制研究[D]. 长沙: 国防科技大学, 2015.
Long W. Researches on crosstalk induced by light in the infrared TDI array detector of PV-HgCdTe[D]. Changsha: National University of Defense Technology, 2015.

[21] (美)贝蒂利瑟·安德森, (美)理查德·安德森. 半导体器件基础[M]. 邓宁, 田立林, 任敏, 译. 北京: 清华大学出版社, 2008: 83-116.
Anderson B L, Anderson R. Fundamentals of semiconductor devices[M]. Deng L, Tian L L, Ren M, Transl. Beijing: Tsinghua University Press, 2008: 83-116.

[22] 江天. 单元光电探测器在连续激光辐照下的响应机理研究[D]. 长沙: 国防科技大学, 2012: 21-22.
Jiang T. Study on response mechanism of element photoelectric detectors irradiated by CW laser[D]. Changsha: National University of Defense Technology, 2012: 21-22.

[23] 陈卫业, 李东升, 姬玉龙, 等. 小像元HgCdTe红外焦平面电串音数值模拟研究[J]. 红外技术, 2018, 40(4): 309-315.
Chen W Y, Li D S, Ji Y L, et al. Research on crosstalk characteristics of small pixel-pitch HgCdTe infrared focal plane arrays[J]. Infrared Technology, 2018, 40(4): 309-315.

[24] 翟永成, 丁瑞军. 320×256大电荷容量的长波红外读出电路结构设计[J]. 红外与激光工程, 2016, 45(9): 0904003.
Zhai Y C, Ding R J. 320 × 256 LW IRFPA ROIC with large charge capacity[J]. Infrared and Laser Engineering, 2016, 45(9): 0904003.

[25] 王巍, 武逶, 白晨旭, 等. 硅PIN光电探测器阵列的串扰分析[J]. 半导体光电, 2013, 34(1): 12-15.
Wang W, Wu W, Bai C X, et al. Analysis on electrical crosstalk of silicon PIN photodiode array[J]. Semiconductor Optoelectronics, 2013, 34(1): 12-15.

[26] 徐江涛, 孙羽, 徐超, 等. 背照式像素电学串扰及其抑制[J]. 中国科技论文, 2013, 8(10): 964-968, 980.
Xu J T, Sun Y, Xu C, et al. Electrical crosstalk and elimination for 4T back-side illuminated pixel[J]. China Science Paper, 2013, 8(10): 964-968, 980.

[27] 张瞳, 林春, 陈洪雷, 等. 金属框结构对碲镉汞红外焦平面调制传递函数的影响[J]. 光学学报, 2018, 38(5): 0504001.
Zhang T, Lin C, Chen H L, et al. Influence of metal frame structure on modulation transfer function of HgCdTe infrared focal plane[J]. Acta Optica Sinica, 2018, 38(5): 0504001.

[28] 陈慧伟, 赵慧洁, 贾国瑞. 红外多光谱相机的图像串扰校正方法[J]. 北京航空航天大学学报, 2015, 41(7): 1337-1342.
Chen H W, Zhao H J, Jia G R. Image crosstalk correction method of the infrared multispectral camera[J]. Journal of Beijing University of Aeronautics and Astronautics, 2015, 41(7): 1337-1342.

Electrical Crosstalk of Photovoltaic HgCdTe Array Detector

Qiao Shuai[1,2,3], Wang Rui[1,2,3*], Hou Xiaocheng[1,2,3]

[1]*College of Advanced Interdisciplinary Studies, National University of Defense Technology, Changsha* 410073, *Hunan, China*;

[2]*Nanhu Laser Laboratory, National University of Defense Technology, Changsha* 410073, *Hunan, China*;

[3]*State Key Laboratory of Pulsed Power Laser Technology, National University of Defense Technology, Changsha* 410073, *Hunan, China*

Abstract

Objective The crosstalk effect has always been one of the challenging issues in detector performance. Due to the increase in the detector array scale and the decrease in pixel center distance, the spatial resolution of the detectors greatly improves, and the crosstalk effect becomes more obvious, with a significant impact on the performance of the detectors. The crosstalk effect considers the problem of signals produced in the target pixel being interfered by some factors and makes other pixels to produce response signals. Crosstalk can be divided into optical crosstalk and electrical crosstalk based on different generation mechanisms. Optical crosstalk refers to the optical factors such as light reflection, refraction, and diffraction that make signals appear in other pixels. Electrical crosstalk refers to the signal response of other pixels due to the diffusion of photogenerated carriers. HgCdTe detector is widely used in both civil and military fields because of its high sensitivity, broad coverage band range, and other advantages. The crosstalk phenomenon exists in array HgCdTe detectors under continuous laser or pulsed laser irradiation, according to a lot of recent studies on the laser irradiation effect of HgCdTe array detectors. Previous research has shown that optical crosstalk is not the primary mechanism driving the response of unirradiated pixels in array devices, and it is inferred that this response is caused by electrical crosstalk. However, the conclusion has not been verified systematically. In this study, a linear HgCdTe array detector is used as the research subject, and we try to explore the mechanism and degree of electrical crosstalk as well as practical strategies for reducing it. In addition, we expect that these findings can have a certain reference value for improving the performance of detectors.

Methods We use COMSOL Multiphysics finite element simulation software to establish a three-dimensional simulation model of a pulsed laser irradiation detector chip and study the crosstalk problem in a laser irradiation linear HgCdTe array detector experiment. Firstly, on the basis of the mechanism of electrical crosstalk caused by the diffusion of photogenerated carriers, the distribution of carrier concentration in the chip under laser irradiation with different energy densities is simulated. It is discovered that the diffusion of photogenerated carriers has a slight direct impact on pixels that are far from the irradiation area. Secondly, the direction of the electric field in the chip is simulated during laser irradiation, and it is discovered that the electric field under laser irradiation points to the common electrode. This electric field will make some photogenerated carriers to move to the common electrode, which will change its voltage and affect the output of the detector. Additionally, the common electrode voltage of the chip is simulated under different energies of laser irradiation, which confirms the conclusion that a decrease in the common electrode voltage can result in a response from every pixel of the detector. Finally, a measure to suppress the crosstalk is suggested. In other words, a three-dimensional isolation trench is designed based on the principle of limiting or reducing the lateral diffusion of photogenerated carriers, and the effect of the suppression of crosstalk is verified by simulation.

Results and Discussions We have discovered that there is a crosstalk phenomenon in pixels far from the irradiation area in the experiment of a 512×1 linear HgCdTe array detector irradiated by a pulsed laser. COMSOL Multiphysics finite element simulation software is used to simulate the carrier concentration distribution in the chip (Fig. 7) and the change of carrier concentration in the center of each pixel with the laser irradiation time (Fig. 8) to study the mechanism of the device′s crosstalk phenomenon. It is discovered that the crosstalk of pixels close to the irradiation area is directly caused by the lateral diffusion of photogenerated carriers along the array alignment, while it has little effect on pixels far from the irradiation area. By simulating the direction of the electric field in the chip (Fig. 9) and the common electrode voltage (Fig. 10), the reason for the response of pixels far from the irradiation area can be fundamentally explained. It is discovered that some photogenerated carriers move to the common electrode under the action of the electric field, which results in the decrease in the common electrode voltage and the rise in all pixels′ responses. The measure of trench isolation to suppress crosstalk (Fig. 11) is established based on the understanding of the device′s electrical crosstalk generation mechanism, and simulation results (Fig. 12) show that the measure has significantly suppressed electrical crosstalk.

Conclusions In view of the crosstalk phenomenon in the laser irradiation linear HgCdTe array detector experiment, the mechanism of the crosstalk is revealed by simulating the carrier concentration distribution, photocurrent, electric field direction, and common electrode voltage in the laser irradiation photosensitive chip in this paper. Research shows that the lateral diffusion of photogenerated carriers along the array alignment directly contributes to the crosstalk of pixels close to the irradiation area, while it has little effect on pixels far from the irradiation area. There is an electric field pointing to the common electrode of chip when it is irradiated by the laser. Under the influence of this electric field, some photogenerated carriers move to the common electrode, which results in the voltage reduction of the common electrode, and then all of the detector′s pixels rise in response. In addition, the measure of electrical crosstalk suppression by trench isolation, which has a significant influence on crosstalk suppression, is proposed based on the mechanism of electrical crosstalk generated by the lateral diffusion of carriers. The problem of crosstalk brought by the common electrode voltage variation can be resolved by changing the circuit design or correcting the output signal. It is necessary to conduct more research on the specific measures.

Key words detectors; HgCdTe; electrical crosstalk; mechanism of crosstalk; trench isolation